

Differential cross sections for intermediate-energy electron scattering from α -tetrahydrofurfuryl alcohol: Excitation of electronic-states

L. Chiari, H. V. Duque, D. B. Jones, P. A. Thorn, Z. Pettifer, G. B. da Silva, P. Limão-Vieira, D. Dufлот, M.-J. Hubin-Franskin, J. Delwiche, F. Blanco, G. García, M. C. A. Lopes, K. Ratnavelu, R. D. White, and M. J. Brunger

Citation: *The Journal of Chemical Physics* **141**, 024301 (2014); doi: 10.1063/1.4885856

View online: <http://dx.doi.org/10.1063/1.4885856>

View Table of Contents: <http://scitation.aip.org/content/aip/journal/jcp/141/2?ver=pdfcov>

Published by the [AIP Publishing](#)

Articles you may be interested in

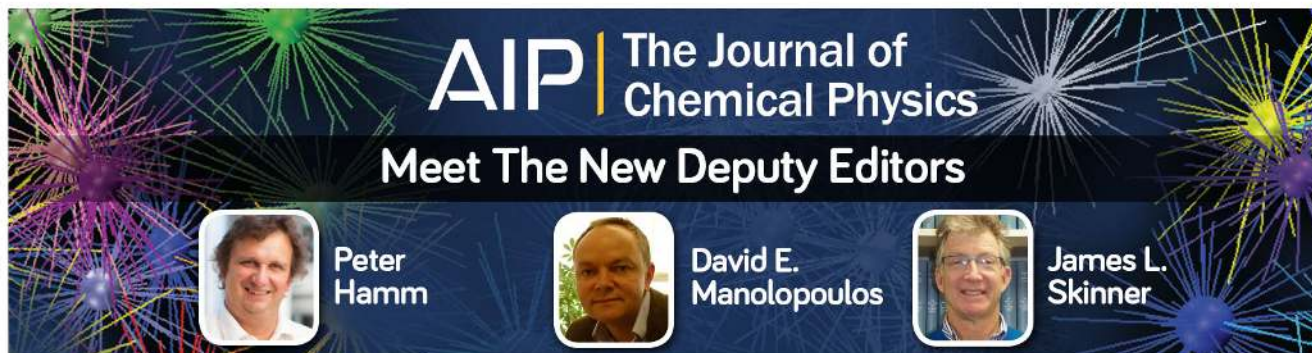
[Intermediate-energy differential and integral cross sections for vibrational excitation in \$\alpha\$ -tetrahydrofurfuryl alcohol](#)
J. Chem. Phys. **140**, 214306 (2014); 10.1063/1.4879779

[Electron scattering from pyrazine: Elastic differential and integral cross sections](#)
J. Chem. Phys. **137**, 204307 (2012); 10.1063/1.4767570

[Absolute electronic excitation cross sections for low-energy electron \(5 – 12 eV \) scattering from condensed thymine](#)
J. Chem. Phys. **122**, 224704 (2005); 10.1063/1.1925610


[Measurement of absolute differential cross sections for the excitation of the \$\pi, \pi^*\$ triplet state of ethene by electron impact at \$0^\circ\$ and \$180^\circ\$](#)
J. Chem. Phys. **106**, 7044 (1997); 10.1063/1.473727


[Vibrational excitation of methane by 15 and 30 eV intermediate-energy electron impact](#)
J. Chem. Phys. **106**, 5990 (1997); 10.1063/1.473263




AIP | The Journal of
Chemical Physics

Meet The New Deputy Editors

 Peter Hamm

 David E. Manolopoulos

 James L. Skinner

Differential cross sections for intermediate-energy electron scattering from α -tetrahydrofurfuryl alcohol: Excitation of electronic-states

L. Chiari,¹ H. V. Duque,^{1,2} D. B. Jones,¹ P. A. Thorn,¹ Z. Pettifer,¹ G. B. da Silva,^{1,3}
 P. Limão-Vieira,⁴ D. Duflot,⁵ M.-J. Hubin-Franskin,⁶ J. Delwiche,⁶ F. Blanco,⁷ G. García,⁸
 M. C. A. Lopes,² K. Ratnavelu,⁹ R. D. White,¹⁰ and M. J. Brunger^{1,9,a)}

¹School of Chemical and Physical Sciences, Flinders University, GPO Box 2100, Adelaide, SA 5001, Australia

²Departamento de Física, Universidade Federal de Juiz de Fora, Juiz de Fora, MG, Brazil

³Universidade Federal de Mato Grosso, Barra do Garças, Mato Grosso, Brazil

⁴Laboratório de Colisões Atômicas e Moleculares, CEFITEC, Departamento de Física, Faculdade de Ciências e Tecnologia, Universidade Nova de Lisboa, 2829-516 Caparica, Portugal

⁵Laboratoire de Physique des Lasers, Atomes et Molécules, UMR CNRS 8523, Université Lille, F-59655 Villeneuve d'Ascq Cedex, France

⁶Département de Chimie, Université de Liège, Institut de Chimie-Bât. B6C, B-4000 Liège 1, Belgium

⁷Departamento de Física Atómica, Molecular y Nuclear, Universidad Complutense de Madrid, Madrid E-28040, Spain

⁸Instituto de Física Fundamental, CSIC, Madrid E-28006, Spain

⁹Institute of Mathematical Sciences, University of Malaya, Kuala Lumpur, Malaysia

¹⁰School of Engineering and Physical Sciences, James Cook University, Townsville, 4810 Queensland, Australia

(Received 11 May 2014; accepted 18 June 2014; published online 8 July 2014)

We report on measurements of differential cross sections (DCSs) for electron impact excitation of a series of Rydberg electronic-states in α -tetrahydrofurfuryl alcohol (THFA). The energy range of these experiments was 20–50 eV, while the scattered electron was detected in the 10°–90° angular range. There are currently no other experimental data or theoretical computations against which we can directly compare the present measured results. Nonetheless, we are able to compare our THFA DCSs with earlier cross section measurements for Rydberg-state electronic excitation for tetrahydrofuran, a similar cyclic ether, from Do *et al.* [J. Chem. Phys. **134**, 144302 (2011)]. In addition, “rotationally averaged” elastic DCSs, calculated using our independent atom model with screened additivity rule correction approach are also reported. Those latter results give integral cross sections consistent with the optical theorem, and supercede those from the only previous study of Milosavljević *et al.* [Eur. Phys. J. D **40**, 107 (2006)]. © 2014 AIP Publishing LLC. [<http://dx.doi.org/10.1063/1.4885856>]

I. INTRODUCTION

It is now well-known that the deposition of energy, from ionising radiation into biological systems, can lead to the production of a significant number of secondary electrons.¹ Those secondary electrons can then undergo inelastic collisions with molecules in the biological media to populate excited states (vibrational and electronic-states), form neutral radical or ion species that can affect the biochemistry or break DNA strands.^{1–3} Electron impact processes hence have the very real capability to cause cellular mutation or necrosis. As a consequence, and particularly over the last decade, there has been a demand for knowledge of low-energy electron interactions with species found in biological systems, in order to try and understand and model the effects induced by radiation.^{3–6} Examples of those systems include tetrahydrofuran (see Refs. 7–9 and references therein), pyrimidine (see Refs. 10–13 and references therein), and pyrazine (see Refs. 14 and 15 and references therein). For the purpose of understanding nano-dosimetry,³ electron-impact differential

cross sections (DCSs), $\sigma_i(E_0, \theta)$, provide the most detail. Differential cross sections, such as we report here, represent the probability that an electron with energy E_0 incident on an atomic or molecular target will scatter into the θ -direction and leave that target in a final state denoted by i . The difficulty in performing experiments of electron scattering from large biomolecules, and in analysing the measured data, to determine absolute DCSs, has, unfortunately, made such experimental data relatively scarce. Furthermore, the large size of biomolecules still makes full-scale *ab initio* scattering calculations, which are generally required to accurately describe low-energy electron interactions with atoms and molecules, typically intractable. Given this historical paucity in the available experimental and theoretical data for the species that constitute biological matter, including the human body, although the situation in the species noted above has certainly improved matters, radiation induced damage to biological matter is often evaluated in water.^{2,3,16,17} Gas phase cross section data may further assist in modelling radiation damage and aid in the interpretation of results from large systems. This creates a pressing need for scattering measurements and the development of theoretical models (benchmarked against data where

^{a)}Electronic mail: Michael.Brunger@flinders.edu.au

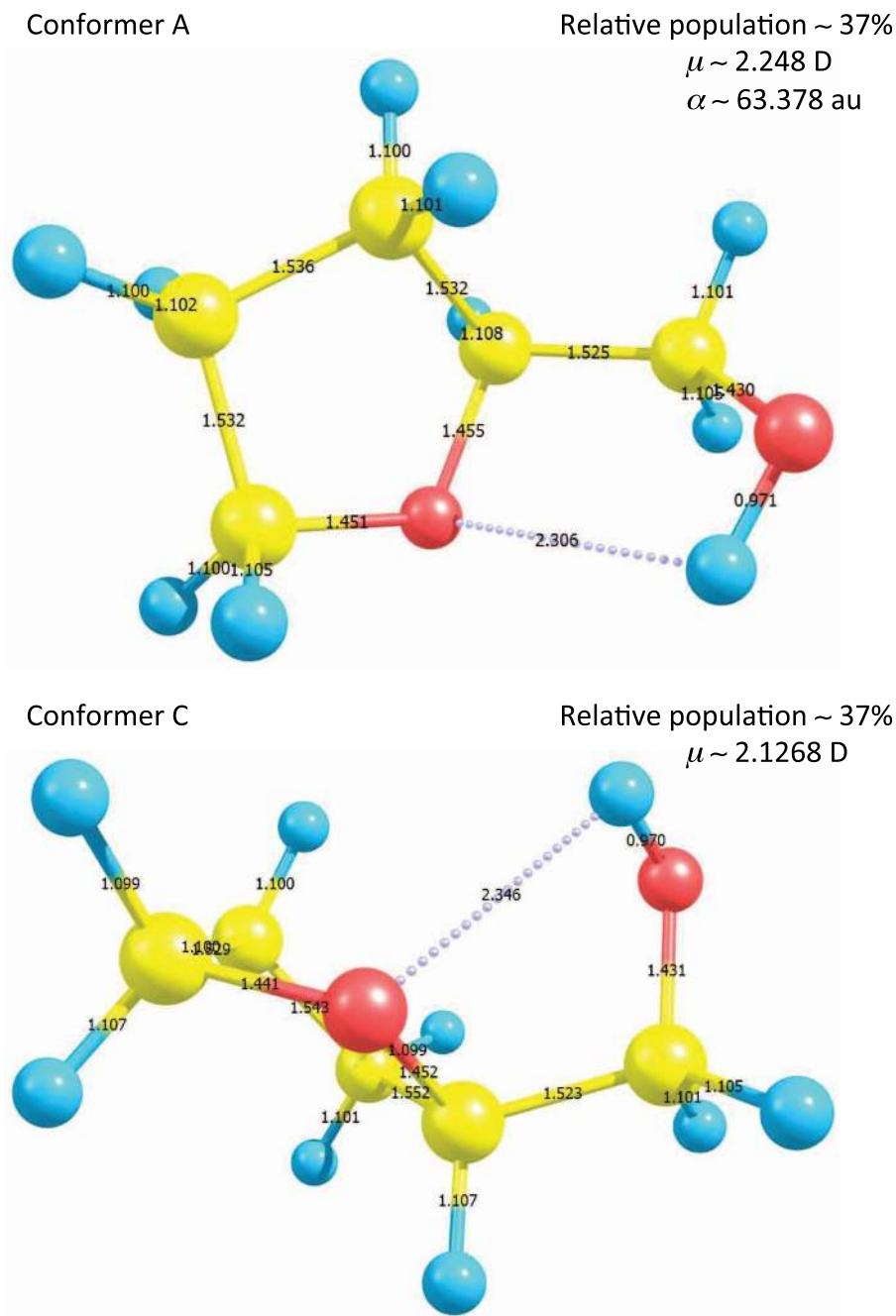


FIG. 1. Representation of the conformer A (top pane) and conformer C (bottom pane) of α -tetrahydrofurfuryl alcohol. Bond lengths are in units of \AA . Calculations were performed at the MP2/aug-cc-pVDZ level. Hydrogen atoms are represented in blue, oxygen in red, and carbon in yellow. Also indicated are their room temperature relative population abundance, dipole moment (μ), and dipole polarisability (α). See Ref. 20 for full details.

possible), that can precisely describe localised electron interactions with matter so that radiation induced damage might accurately be described. Note that the efficacy of using gas phase collision data for charged-particle track simulations in soft matter, has been addressed by White and Robson.¹⁸

α -tetrahydrofurfuryl alcohol (THFA; $C_5H_{10}O_2$) is an excellent analogue moiety for the DNA backbone sugar deoxyribose (see Figure 1 in Bellm *et al.*¹⁹ and Fig. 1 of this paper). As a consequence, our group has conducted a series of gas phase studies on its absolute photoabsorption cross section and photoionisation behaviour,²⁰ a quantum chemical investigation of its excited electronic-state spectroscopy,²⁰ abso-

lute DCS and integral cross section (ICS) measurements for electron-impact vibrational excitation²¹ and a preliminary report describing ICS measurements for electron excitation of a series of its Rydberg electronic-states.²² In that latter paper we also reported theoretical results from our independent atom model (IAM) with screened additivity rule (SCAR) correction computations, for the total cross section (TCS), elastic ICS, inelastic ICS (all discrete electronic-states and neutral dissociation), and the total ionisation ICS.²² Here, we conclude this work by reporting the corresponding Rydberg electronic-state DCSs and our IAM-SCAR elastic DCSs. Note that a full summary of previous investigations for photon, electron, and

positron scattering from THFA can be found in Refs. 20–22 and so we do not again repeat that detail here. Irrespective of our desire to provide accurate cross section data for charged-particle track simulation studies,^{2–5,16} as well as to assist in the benchmarking of theory, THFA possesses several intrinsic physico-chemical properties which, from our experience with other scattering systems,^{23–26} are anticipated to play important roles in the collision dynamics. Specifically, THFA has a strong permanent dipole moment of magnitude ~ 2 D²⁷ and a significant dipole polarisability of ~ 70.18 a.u.²⁸ Note that these values are consistent with those from our own MP2/cc-pVTZ level calculations²⁰ for the main A and C conformers in THFA. We therefore also wished to investigate if those physico-chemical properties manifested themselves in the behaviour of the electronic-state DCSs, in particular in their angular distributions, of THFA.

Details of our measurement and analysis procedures are given in Sec. II. Thereafter, a brief description of our IAM-SCAR approach is provided, before in Sec. IV our experimental results are presented and discussed. Finally, in Sec. V, some concluding remarks are drawn.

II. EXPERIMENTAL DETAILS AND ANALYSIS PROCEDURES

To determine absolute DCSs for electron impact excitation of the series of Rydberg electronic-states²⁶ in THFA, we begin with measurements of electron energy loss spectra (EELS). A typical example of an EELS from this study is given in Fig. 2, which also indicates the excitation energies for the electronic spectrum of the isomers A and C (see Fig. 1) of THFA as calculated by Limão-Vieira *et al.*²⁰ Those energy loss spectra were collected with an apparatus based at Flinders University, as originally described in Brunger and Teubner.²⁹ Nonetheless, to ensure this paper is self-contained, we note that in this work a monochromated beam of 20–50 eV elec-

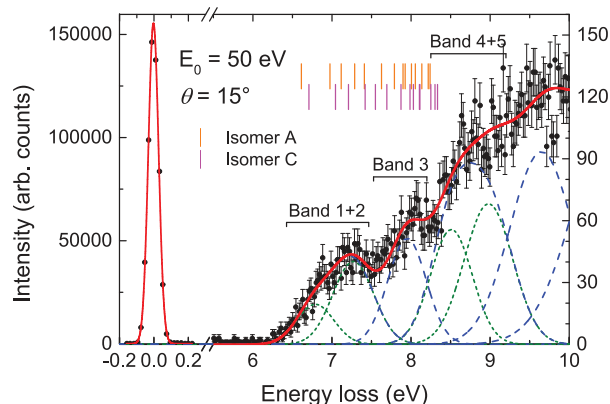


FIG. 2. Typical electron energy loss spectrum of THFA at $E_0 = 50$ eV, $\theta = 15^\circ$. The overall spectral deconvolution fit is denoted by the solid red line, while the fits to the various bands are also shown by the dashed lines. The short-dashed green lines represent spectral features of individual spectral deconvolution bands (bands 1–5, respectively), while the blue longer dashes indicate the bands which are subsequently combined together (i.e., bands 1+2, band 3, and bands 4+5).²² Also indicated are the excitation energies for the electronic spectrum of the isomers A and C of THFA as calculated by Limão-Vieira *et al.*²⁰

trons, with a typical current of 1–3 nA, was incident on an orthogonal beam of THFA molecules. That molecular beam was formed by allowing vapour from a high-purity THFA sample (Sigma-Aldrich, 99% assay) to effuse through a single capillary of 0.7 mm internal diameter. Unfortunately, at room temperature the vapour pressure of THFA is rather low ($P = 186$ Pa $\equiv 1.4$ Torr at 25 °C³⁰), so that we needed to warm our sample to ~ 55 °C in order to produce sufficient vapour at the interaction region. Note that to facilitate a stable THFA beam, the gas handling lines and vacuum chamber were heated to ~ 60 °C. Under the stable beam conditions maintained during the EELS measurements, the THFA vacuum chamber pressure was always kept below 1×10^{-5} Torr to ensure multiple scattering effects could be neglected. In the present investigations the overall instrumental energy resolution was ~ 65 meV (FWHM), while the scattered electron angle (θ) range was 10° – 90° . EELS were collected at each scattering angle and incident electron energy (20, 30, 40, and 50 eV) by recording the number of scattered electrons detected at each energy loss value. The true electron count rate at each given energy loss was recorded using a multichannel scaler synchronised to a linear voltage ramp that varied the detected energy loss between -0.2 and 10 eV. In this way a given EELS is built up by continually scanning over the selected range of energy loss values, so that the effect of any variations in the target beam flux or incident electron current on an EELS is minimised. In general, at each E_0 and θ , the EELS were measured 2–4 times to ensure reproducibility of the inelastic to elastic ratios (see below) to within the experimental uncertainty.

In Ref. 22 we previously outlined our spectral deconvolution approach, and the basis^{20,22} for that approach, and so we also do not repeat that detail again here. Rather, we simply note that the various EELS were deconvoluted, using a standard least-squares fitting procedure, into contributions arising from each individual or unresolved combination of excited electronic-states. Either one or two Gaussian functions were employed to describe the spectral profiles for each resolvable inelastic feature and the elastic scattering peak. The positions and widths of the Gaussians for each inelastic feature were established through a consideration of the experimental photoabsorption spectrum²⁰ and our experimental energy resolution. The peak energies and indicative spectral widths of the electronic-state features that we used in our spectral deconvolutions, for each of the five bands identified in the EELS for THFA, are given in Table 1 of Duque *et al.*,²² with those bands of states and their components from the deconvolution being indicated in Fig. 2. The detailed quantum chemical calculations given by Limão-Vieira *et al.*,²⁰ also permit us to believe that bands 1+2, 3, and 4+5 in Fig. 2 are largely composed of transitions of Rydberg character for the 4 conformers expected to be present in our THFA sample. Specifically, *ab initio* calculations were performed by Limão-Vieira *et al.*²⁰ to determine the geometry and excitation energies of the neutral molecules (see Tables 3–8 in Ref. 20), using the MOLPRO program.³¹ The geometry was optimised at the MP2 level using Dunning’s cc-pVTZ and aug-cc-pVDZ atomic orbitals basis sets.³² Six conformers, labelled A–F, were studied in that investigation. The electronic spectra were computed

TABLE I. Present experimental electronic-to-elastic ratios ($\times 10^{-3}$), differential cross sections ($\times 10^{-23}$ m²/sr), and related uncertainty (%) for electron-impact excitation of the Rydberg-states of THFA found in bands 1+2 (energy loss range 6.2–7.6 eV).

θ (°)	20 eV			30 eV			40 eV			50 eV		
	Ratio	DCS	Uncert.	Ratio	DCS	Uncert.	Ratio	DCS	Uncert.	Ratio	DCS	Uncert.
10	3.93	265.21	27.5									
15	3.50	117.08	25.1	3.31	96.32	23.3	3.25	106.85	24.0	3.26	103.02	24.4
20	3.26	45.90	27.8	3.80	51.76	23.6	4.84	64.07	24.9	5.86	75.85	24.1
30	5.22	44.74	25.2	4.87	37.21	28.6	6.21	40.86	27.2	5.04	24.13	35.2
40	5.86	34.45	24.9	5.58	19.52	27.0	6.38	16.33	27.0	5.37	12.20	38.0
50	6.14	20.81	23.2	6.13	13.36	25.2	6.63	12.13	27.7	4.29	6.41	47.4
60	6.74	17.22	31.8	6.65	11.81	25.2	6.55	8.09	31.8	6.58	5.73	40.8
70	7.90	17.85	28.4	8.94	11.92	30.3	7.21	6.08	29.4	6.69	3.92	32.4
80	8.95	17.45	29.0	9.93	9.73	28.9	7.72	4.86	26.5	5.66	2.54	42.0
90	9.25	14.15	27.2	10.82	8.36	25.9	8.02	4.15	31.6	6.72	2.61	37.6

at the equation of motion-coupled cluster with singles and doubles (EOM-CCSD) level.³³ For that, the aug-cc-pVDZ basis set was used, and a set of (6s 6p 5d) diffuse functions, taken from Kaufmann *et al.*,³⁴ was added on the C₂ carbon atom for a better description of the Rydberg states. Full details of the electronic-state assignments can also be found in Tables 3–8 of Limão-Vieira *et al.*²⁰ Note that the calculated energies of the excited electronic-states of the two most populated A and C conformers²⁰ (estimated to make up ~74% of our THFA sample) are also shown in Fig. 2. Further note that the electronic-state spectroscopy, at least qualitatively, of THFA appears to be very similar to that for the structurally related compound tetrahydrofuran (THF).⁸ The amplitudes of the Gaussian functions were now varied in a least-squares fitting procedure to provide the best fit to the measured spectra (see Fig. 2). The ratio (R) of the area under the fitting function for each i th inelastic band to that under the elastic feature, at each E_0 and θ , is simply related to the ratio of the differential cross sections from:

$$R_i(E_0, \theta) = \frac{\sigma_i(E_0, \theta)}{\sigma_0(E_0, \theta)}. \quad (1)$$

Note that Eq. (1) is only valid if the transmission efficiency of the analyser remains constant over the energy loss and angular range studied, or is at least well characterised. Following

an approach similar to that of Allan,³⁵ an additional focusing lens (synchronised to the voltage ramp) was also employed to minimise variations in the angular transmission efficiency for electrons detected with different energy losses. Our results suggest that the efficiency is unity, to within an uncertainty of 20%. The results for the present measured R_i , for each of bands 1+2, 3, and 4+5 of Rydberg states, are given in the first column of Tables I–III, respectively.

It should be apparent from Eq. (1) that the product of $R_i \times \sigma_0$ then gives the required Rydberg-band differential cross section provided σ_0 is known. In this work, and in our previous electron–THFA papers,^{21,22} we have utilised our IAM-SCAR elastic differential cross sections at 20, 30, 40, and 50 eV (see Sec. III for details) to set the absolute inelastic scale at each E_0 and θ , with a selection of those theoretical elastic results being plotted in Fig. 3. It is clear from Fig. 3 that each of these rotationally averaged elastic DCSs are very strongly forward peaked in magnitude as you go to smaller scattered electron angles. Note that no measured elastic DCSs currently exist in the literature to compare our computations against and thus possibly validate them. However, there are several examples of elastic DCS for other species (e.g., Refs. 36–38) where the comparison between the IAM-SCAR DCS and independent measurements is very good down to energies of ~20 eV. There are also cases where such a

TABLE II. Present experimental electronic-to-elastic ratios ($\times 10^{-3}$), differential cross sections ($\times 10^{-23}$ m²/sr), and related uncertainty (%) for electron-impact excitation of the Rydberg-states of THFA found in band 3 (energy loss range 7.6–8.2 eV).

θ (°)	20 eV			30 eV			40 eV			50 eV		
	Ratio	DCS	Uncert.	Ratio	DCS	Uncert.	Ratio	DCS	Uncert.	Ratio	DCS	Uncert.
10	2.13	143.55	29.8									
15	1.94	65.11	25.7	2.41	70.21	24.4	2.45	80.72	23.7	2.73	86.29	23.8
20	2.05	28.86	29.5	3.20	43.51	24.3	3.45	45.71	24.3	4.24	54.80	24.2
30	3.57	30.59	27.7	3.31	25.29	29.8	4.86	31.99	26.4	4.51	21.57	33.4
40	3.83	22.55	24.5	4.90	17.14	24.4	4.58	11.71	28.1	4.10	9.32	35.9
50	4.33	14.66	23.6	4.62	10.07	24.9	5.01	9.17	27.6	4.23	6.31	36.0
60	4.89	12.48	30.4	4.93	8.75	26.9	4.88	6.02	33.2	4.68	4.08	37.2
70	4.83	10.92	30.0	7.07	9.43	26.0	4.99	4.21	33.5	4.40	2.57	30.5
80	5.68	11.06	29.2	7.95	7.80	29.4	5.90	3.72	25.9	5.34	2.39	34.4
90	6.17	9.44	29.5	8.01	6.20	25.3	6.22	3.22	30.6	4.86	1.89	35.8

TABLE III. Present experimental electronic-to-elastic ratios ($\times 10^{-3}$), differential cross sections ($\times 10^{-23}$ m²/sr), and related uncertainty (%) for electron-impact excitation of the Rydberg-states of THFA found in bands 4+5 (energy loss range 8.2–9.3 eV).

θ (°)	20 eV			30 eV			40 eV			50 eV		
	Ratio	DCS	Uncertainty	Ratio	DCS	Uncertainty	Ratio	DCS	Uncertainty	Ratio	DCS	Uncertainty
10	5.52	373.21	26.4									
15	5.44	182.10	24.2	6.44	187.60	23.3	6.59	216.98	23.0	7.49	236.96	23.2
20	5.64	79.23	32.9	8.15	110.93	23.8	9.62	127.46	23.3	12.55	162.40	23.1
30	10.43	89.36	32.4	10.89	83.22	25.8	13.44	88.47	24.2	13.80	66.07	26.2
40	11.16	65.62	23.7	13.89	48.60	23.3	13.93	35.64	24.5	13.31	30.22	27.0
50	13.03	44.16	22.6	14.89	32.47	23.3	14.34	26.24	24.3	11.38	16.99	29.5
60	13.43	34.31	25.7	17.01	30.19	23.1	16.88	20.84	25.1	14.42	12.56	28.2
70	15.33	34.64	25.5	18.60	24.79	26.2	17.69	14.91	24.5	16.49	9.65	25.2
80	17.14	33.40	24.4	29.13	28.55	32.1	20.52	12.93	23.5	17.16	7.69	26.9
90	20.04	30.64	24.0	24.74	19.13	23.9	22.23	11.51	24.7	17.49	6.80	26.6

comparison is only accurate to energies of ~ 50 eV and above.^{24,26,39} Nonetheless, for the chemically similar and fellow cyclic ether species THF, the IAM-SCAR is found to be in good accord with available measurements^{40,41} at energies of 20 eV and above. We are therefore quite confident it will be similarly applicable here. There is, however, one caveat to this last statement. Returning to Fig. 3 then on closer inspection each of the elastic THFA DCS exhibit a small “kink” in their angular distribution, with the scattering angle at which it occurs being energy dependent. This “kink” arises due to a normalisation procedure in the IAM-SCAR which ensures that integral cross sections derived from integration of the molecular DCS are entirely consistent with those determined from the atomic ICS in conjunction with the optical theorem⁴² (see Sec. III). As a consequence, for scattering angles at 10° and 15° (i.e., in the region relevant to our ratio measurements) and on the basis of what we find in THF when comparing experiment and the IAM-SCAR results our calculated THFA elastic DCS are scaled up using the THF experimental DCS to theory DCS ratio at 10° or 15° and at each E_0 . While this is actually a relatively small correction, we believe it was important to make it. The results of our inelastic DCSs, and their associated uncertainties, are listed in Tables I–III for the electron

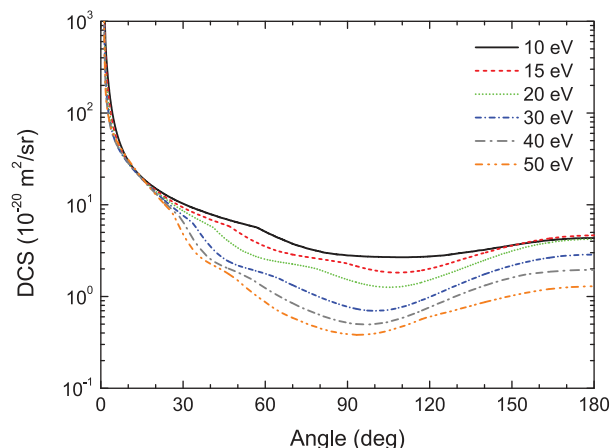


FIG. 3. Present IAM-SCAR elastic differential cross sections ($\times 10^{-20}$ m²/sr), averaged over the rotational excitations, are shown at selected impact energies in the range 10–50 eV.

impact excited Rydberg-states found in bands 1+2, band 3, and bands 4+5. These data are also plotted in Fig. 4.

Finally, we have paid some attention to the identification and quantification of all possible sources of error in this study. Here the statistical errors associated with the scattering intensity measurements (i.e., the EELS) are small ($\leq 2\%$). An additional error due to our analyser transmission calibration ($\sim 20\%$) must also be considered. While the inherent uncertainty in our IAM-SCAR elastic DCS calculations are negligible, we have found from past experience^{36–38,40} that it can often reproduce the data to 10% or better. Hence a 10% uncertainty on our elastic DCS has been incorporated into our analysis. Another important source of possible error is that associated with the numerical deconvolution of the energy-loss spectra, so that an allowance for this is also made in the overall DCS uncertainties. When all these components are combined in quadrature, the errors on our DCS are found to be in the range 23%–47% with the precise error depending on the energy, scattering angle and Rydberg band in question.

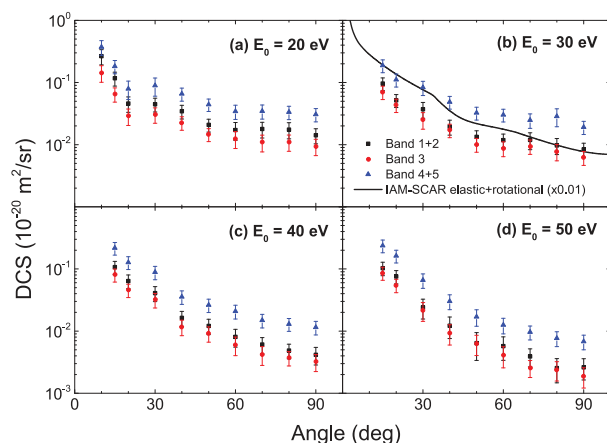


FIG. 4. Differential cross sections ($\times 10^{-20}$ m²/sr) for the electronic excitation of THFA at different incident electron energies: (a) 20 eV, (b) 30 eV, (c) 40 eV, and (d) 50 eV. Shown in each panel are the DCSs for: (■) bands 1+2 (energy loss range 6.2–7.6 eV), (●) band 3 (7.6–8.2 eV), (▲) bands 4+5 (8.2–9.3 eV). Also plotted in (b) is the IAM-SCAR elastic DCS (—) averaged over the rotational excitations ($\times 0.01$) at 30 eV impact energy.

III. THEORY

Our IAM-SCAR approach has already been extensively used to calculate electron scattering cross sections for a wide variety of atomic (see, e.g., Ref. 43) and molecular targets (see, e.g., Refs. 24, 26, 36–41, and 44) and over a broad energy range. Therefore, we only précis the salient points of this method here. The initial subjects of our calculations are the individual atoms that constitute the target molecule, i.e., carbon (C), hydrogen (H), and oxygen (O) in this case. Our atomic optical model is based on a potential scattering approach, where the complex potential $V(r)$ is given by

$$V(r) = V_s(r) + V_{\text{ex}}(r) + V_p(r) + iV_a(r). \quad (2)$$

Here $V_s(r)$ is the usual Hartree potential of the target, $V_{\text{ex}}(r)$ represents the exchange interaction of Riley and Truhlar,⁴⁵ $V_p(r)$ is the dipole polarisation potential of Zhang *et al.*⁴⁶ and $V_a(r)$ is the imaginary absorption potential of Staszewska *et al.*⁴⁷ Owing to the final term in Eq. (2), the optical model potential method yields complex phase shifts which are then employed to calculate the differential and integral cross sections for elastic and inelastic scattering. Note that for this paper only the elastic DCS are important.

To calculate the cross sections for molecules, we follow the IAM by applying a coherent addition procedure known as the additivity rule (AR). In this approach, the molecular scattering amplitude is derived from the sum of all the relevant atomic amplitudes, including the phase coefficients, therefore leading to the DCSs for the molecule in question. A limitation with the AR is that no molecular structure is considered, so that it is really only applicable when the incident electrons are so fast ($E_0 \geq 100$ eV) that they effectively only see the target molecule as a sum of the individual atoms. To reduce the effect of that limitation, we introduced the SCAR method⁴⁸ which considers the geometry of the relevant molecule (atomic positions and bond lengths) by employing some screening coefficients. With this correction, as we noted earlier, the range of validity might be extended down to incident energies of ~ 20 eV.

The IAM-SCAR approach discussed above does not account for vibrational and rotational excitations. However, for polar molecules such as THFA, additional dipole-induced excitation cross sections can be calculated following Jain.⁴⁹ In that approach, rotational excitation DCSs for a free electric dipole are calculated in the framework of the first Born approximation. These results can then be incorporated into our IAM-SCAR calculation in an incoherent manner, simply by adding up the cross sections as independent channels. As in general the experiments measure rotationally averaged elastic DCS, the Born-dipole rotational cross sections are added to the “pure” elastic IAM-SCAR DCS to ensure the experimental conditions are accounted for. A selection of our DCS results from the current computations is given in Fig. 3.

IV. RESULTS AND DISCUSSION

In Tables I–III we, respectively, present the current measured differential cross sections for electron impact exci-

tation of the Rydberg-states found in bands 1+2, band 3, and bands 4+5 in THFA. Also shown in these tables are the associated overall errors on those DCSs, which are reported to the one standard deviation level. All these data are also plotted in Fig. 4, at each of 20 eV, 30 eV, 40 eV, and 50 eV. In Fig. 4(b) we additionally plot our rotationally averaged IAM-SCAR elastic DCS, scaled by a factor of 0.01. This enables us to, at 30 eV, compare the angular distributions of the electronic-states to that for elastic scattering and to indicate just how much smaller in magnitude the electronic-state excitation cross sections are relative to that for the elastic channel.

There are several general trends that emerge from a consideration of the differential cross section data in Fig. 4. First, at each energy, the shapes of the inelastic angular distributions of each of the Rydberg bands of electronic-states, at least to within the stated errors, are almost identical. This is consistent with results for Rydberg-state excitation from our earlier study into electron impact scattering from nitric oxide (NO).^{50,51} Second, again at each energy and for all the Rydberg bands, the angular distributions (shapes) are strongly peaked in magnitude as you go to smaller scattered electron angles. This behaviour is consistent with the important role played by both the permanent dipole moment and dipole polarisability of the target in the dynamics of this scattering system. Finally, it is clear that in each case the magnitudes of the DCSs for bands 4+5 are significantly larger than the DCSs for bands 1+2 which are in turn a little larger in magnitude than those for band 3. This latter observation is entirely consistent with the EELS data in Fig. 2. As we noted above, in Fig. 4(b) we have also included the rotationally averaged elastic DCS from our IAM-SCAR calculations (scaled by a factor of 0.01). Here we see that while the elastic and inelastic DCSs are similar in shape, there is a subtle difference between them. Namely, the magnitudes of the DCSs at middle angles for the inelastic excitation processes are relatively stronger, compared to those at forward angles, than in the elastic scattering case. It is known that the phenomenon of electron exchange tends to make a larger contribution to the collision cross sections at middle and backward angles, compared to forward angles, so that perhaps the result in Fig. 4(b) suggests that exchange is relatively more important in describing the inelastic processes than the elastic process in THFA. This is a little speculative on our part, theory being required for a quantitative explanation of this point.

In Fig. 5 we now compare the DCSs for THFA and THF,⁸ for electron impact excitation of their corresponding Rydberg bands 1+2 and band 3 electronic-states. Here we find that for scattering angles less than $\sim 30^\circ$, the DCSs of bands 1+2 and band 3 in both THFA and THF, to within their errors, are very similar in magnitude. Note that this statement holds at each of 20, 30, and 50 eV incident energies. Recall that THFA and THF have similar magnitude permanent dipole moments (μ).²² Therefore, perhaps the above observation might be explained in terms of the dipole moment dominating the scattering dynamics in this forward scattered electron angular range, where all the cross sections are strongly peaked in magnitude, so that the similar THFA and THF magnitudes

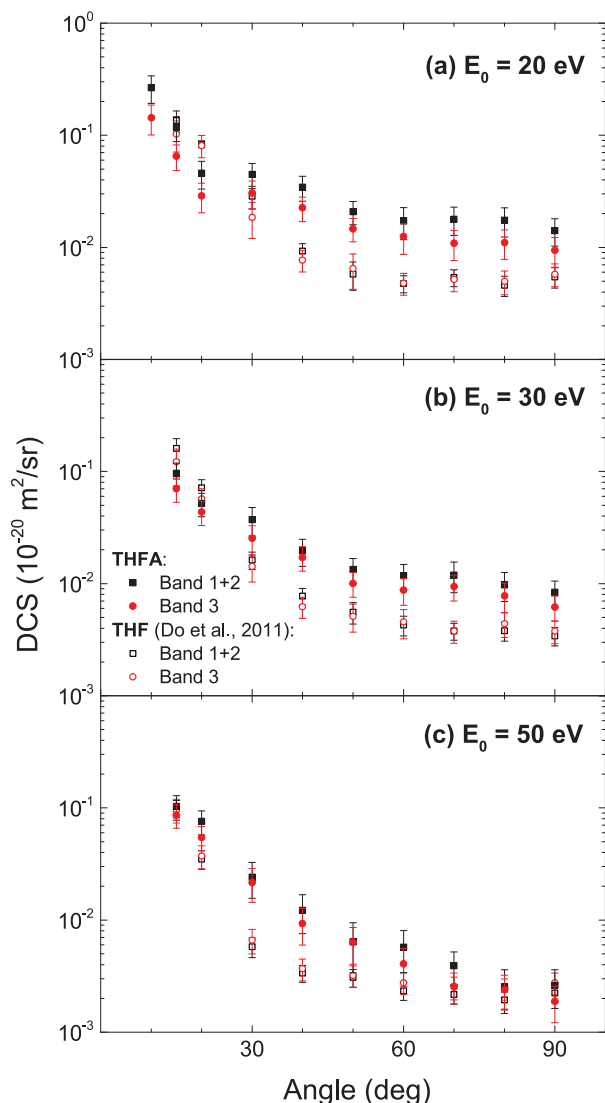


FIG. 5. Comparison of the present differential cross sections ($\times 10^{-20} \text{ m}^2/\text{sr}$) for the electronic excitation of THFA to those of Do *et al.*⁸ for the structurally similar molecule THF at the common impact energies: (a) 20 eV, (b) 30 eV and (c) 50 eV. Shown in each panel are the DCSs for similar excitation ranges: (■) THFA, bands 1+2; (●) THFA, band 3; (□) THF, bands 1+2; (○) THF, band 3.

echoes their similar values for μ . At scattering angles greater than and equal to about 30° , again at each energy plotted in Fig. 5, the magnitudes for the relevant THFA DCS Rydberg bands are typically larger than those of THF. As the dipole polarisability is, to first order, an indicator for the extent of the molecular charge cloud and, in a semi-classical sense, you are more likely to “hit” a larger target than a smaller target (i.e., have a larger cross section), perhaps this behaviour at middle angles is a representative of the THFA dipole polarisability being quite a bit larger than that for THF ($\alpha \sim 47.08 \text{ a.u.}$ ⁵²). In this context, we are therefore suggesting that the middle angle inelastic scattering dynamics are being more strongly influenced by the target dipole polarisability. Note, however, a quantitative understanding for the comparative THFA and THF inelastic DCS behaviour in Fig. 5 also awaits detailed theoretical calculations for both species.

V. CONCLUSIONS

We have reported on differential cross section measurements for electron impact excitation of electronic-states in THFA in the energy range 20–50 eV. No independent theory or measured data are currently available to directly compare against those results, although we hope this work stimulates such further studies. The shapes of the angular distributions of the present DCSs, at each energy studied, are consistent with dipole-effects playing a major role in governing the collision dynamics in this scattering system. We have also presented ‘rotationally’ averaged IAM-SCAR elastic DCSs, that supercede some earlier results,⁵³ which played a pivotal role in setting the absolute cross section scales on our inelastic results. When we compared the present THFA electronic-state DCSs to corresponding results in the structurally similar cyclic ether THF, at the relevant energies and for Rydberg bands of states where such a comparison was possible, we found subtle differences between them. In particular, for $\theta \geq 30^\circ$ the magnitude of the THFA DCSs were usually larger than those for THF with the quantitative explanation for this observation not yet being clear. Nonetheless, on the basis of this comparison, we speculated that while the forward angle scattering dynamics were largely being driven by the species respective permanent dipole moments, the observed middle and more backward angle behaviour might reflect the role of their dipole polarisabilities. This paper represents the final in a series of papers that looked at cross sections for vibrational²¹ and electronic-state^{20,22} excitation processes in THFA. Extensive electronic-structure computations were also reported.²⁰ Together with that earlier work, here we have gone one step further in fulfilling one of the rationales behind these investigations. Namely, constructing a THFA data base that might be employed for charged-particle track simulation purposes. We note that this latter aim has been further enhanced by the recent total ionisation cross section data from Bull *et al.*⁵⁴

ACKNOWLEDGMENTS

The authors wish to thank the Australian (through the Australian Research Council), Belgian, Brazilian (through CNPq, CAPES, and FAPEMIG), French (CaPPA project from ANR through the PIA under Contract No. ANR-10-LABX-005), Malaysian, Portuguese (PEst-OE/FIS/UI0068/2014 and PTDC/FIS-ATO/1832/2012 through FCT-MEC) and Spanish (Ministerio de Economía y Competitividad under Project No. FIS2012-31230) funding agencies who financially supported various aspects of this work. One of us (M.J.B.) acknowledges the University of Malaya for his “Distinguished Visiting Professorship” and CNPq for his “Special Visiting Professorship,” while another (D.B.J.) thanks the ARC for his Discovery Early Career Research Award. Finally, H.V.D. thanks the Science Without Borders scheme that enabled him to visit and study in Australia. We all thank Dr. L. Campbell for his assistance in preparing this manuscript.

¹B. Boudaiffa, P. Cloutier, D. Hunting, M. A. Huels, and L. Sanche, *Science* **287**, 1658 (2000).

²A. Muñoz, F. Blanco, G. García, P. A. Thorn, M. J. Brunger, J. P. Sullivan, and S. J. Buckman, *Int. J. Mass Spectrom.* **277**, 175 (2008).

- ³A. G. Sanz, M. C. Fuss, A. Muñoz, F. Blanco, P. Limão-Vieira, M. J. Brunger, S. J. Buckman, and G. García, *Int. J. Radiat. Biol.* **88**, 71 (2012).
- ⁴Z. Lj. Petrović, S. Marjanović, S. Dujko, A. Banković, G. Malović, S. Buckman, G. García, R. White, and M. Brunger, *Appl. Radiat. Isot.* **83**, 148 (2014).
- ⁵R. D. White, W. Tattersall, G. Boyle, R. E. Robson, S. Dujko, Z. Lj. Petrović, A. Banković, M. J. Brunger, J. P. Sullivan, S. J. Buckman, and G. García, *Appl. Radiat. Isot.* **83**, 77 (2014).
- ⁶I. Plante and F. A. Cucinotta, *New J. Phys.* **10**, 125020 (2008).
- ⁷C. J. Colyer, V. Vizcaino, J. P. Sullivan, M. J. Brunger, and S. J. Buckman, *New J. Phys.* **9**, 41 (2007).
- ⁸T. P. T. Do, M. Leung, M. Fuss, G. García, F. Blanco, K. Ratnavelu, and M. J. Brunger, *J. Chem. Phys.* **134**, 144302 (2011).
- ⁹N. A. Garland, M. J. Brunger, G. García, J. de Urquijo, and R. D. White, *Phys. Rev. A* **88**, 062712 (2013).
- ¹⁰P. Palihawadana, J. Sullivan, M. Brunger, C. Winstead, V. McKoy, G. García, F. Blanco, and S. Buckman, *Phys. Rev. A* **84**, 062702 (2011).
- ¹¹D. B. Jones, S. M. Bellm, F. Blanco, M. Fuss, G. García, P. Limão-Vieira, and M. J. Brunger, *J. Chem. Phys.* **137**, 074304 (2012).
- ¹²Z. Mašín, J. D. Gorfinkiel, D. B. Jones, S. M. Bellm, and M. J. Brunger, *J. Chem. Phys.* **136**, 144310 (2012).
- ¹³M. C. Fuss, A. G. Sanz, F. Blanco, J. C. Oller, P. Limão-Vieira, M. J. Brunger, and G. García, *Phys. Rev. A* **88**, 042702 (2013).
- ¹⁴P. Palihawadana, J. P. Sullivan, S. J. Buckman, and M. J. Brunger, *J. Chem. Phys.* **137**, 204307 (2012).
- ¹⁵A. G. Sanz, M. C. Fuss, F. Blanco, J. D. Gorfinkiel, D. Almeida, F. Ferreira da Silva, P. Limão-Vieira, M. J. Brunger, and G. García, *J. Chem. Phys.* **139**, 184310 (2013).
- ¹⁶M. C. Fuss, A. G. Sanz, A. Muñoz, F. Blanco, M. J. Brunger, S. J. Buckman, P. Limão-Vieira, and G. García, *Appl. Radiat. Isot.* **83**, 159 (2014).
- ¹⁷F. Blanco, A. Muñoz, D. Almeida, F. Ferreira da Silva, P. Limão-Vieira, and G. García, *Int. J. Mass Spectrom.* **365–366**, 287 (2014).
- ¹⁸R. D. White and R. E. Robson, *Phys. Rev. Lett.* **102**, 230602 (2009).
- ¹⁹S. M. Bellm, J. D. Builth-Williams, D. B. Jones, H. Chaluvadi, D. H. Madison, C. G. Ning, F. Wang, X. Ma, B. Lohmann, and M. J. Brunger, *J. Chem. Phys.* **136**, 244301 (2012).
- ²⁰P. Limão-Vieira, D. Duflo, M.-J. Hubin-Franskin, J. Delwiche, S. V. Hoffmann, L. Chiari, D. B. Jones, M. J. Brunger, and M. C. A. Lopes, "Electronic states of Tetrahydrofurfuryl Alcohol (THFA) as studied by VUV spectroscopy and *ab initio* calculations," *J. Phys. Chem. A* (published online).
- ²¹H. V. Duque, L. Chiari, D. B. Jones, Z. Pettifer, G. B. da Silva, P. Limão-Vieira, F. Blanco, G. García, R. D. White, M. C. A. Lopes, and M. J. Brunger, *J. Chem. Phys.* **140**, 214306 (2014).
- ²²H. V. Duque, L. Chiari, D. B. Jones, P. A. Thorn, Z. Pettifer, G. B. da Silva, P. Limão-Vieira, D. Duflo, M.-J. Hubin-Franskin, J. Delwiche, F. Blanco, G. García, M. C. A. Lopes, K. Ratnavelu, R. D. White, and M. J. Brunger, *Chem. Phys. Lett.* **608**, 161 (2014).
- ²³H. Kato, H. Kawahara, M. Hoshino, H. Tanaka, M. J. Brunger, and Y.-K. Kim, *J. Chem. Phys.* **126**, 064307 (2007).
- ²⁴J. R. Brunton, L. R. Hargreaves, S. J. Buckman, G. García, F. Blanco, O. Zatsarinny, K. Bartschat, and M. J. Brunger, *Chem. Phys. Lett.* **568–569**, 55 (2013).
- ²⁵D. B. Jones, S. M. Bellm, P. Limão-Vieira, and M. J. Brunger, *Chem. Phys. Lett.* **535**, 30 (2012).
- ²⁶J. R. Brunton, L. R. Hargreaves, T. M. Maddern, S. J. Buckman, G. García, F. Blanco, O. Zatsarinny, K. Bartschat, D. B. Jones, G. B. da Silva, and M. J. Brunger, *J. Phys. B* **46**, 245203 (2013).
- ²⁷P. Mozejko, A. Domaracka, E. Ptasińska-Denga, and C. Szmytkowski, *Chem. Phys. Lett.* **429**, 378 (2006).
- ²⁸C. Szmytkowski and E. Ptasińska-Denga, *J. Phys. B* **44**, 015203 (2011).
- ²⁹M. J. Brunger and P. J. O. Teubner, *Phys. Rev. A* **41**, 1413 (1990).
- ³⁰CERI, "Vapour pressure study of tetrahydrofurfuryl alcohol," CAS No. 97-99-4, Test No. 805283 (Chemicals Evaluation and Research Institute, Tokyo, Japan, 2004).
- ³¹H.-J. Werner, P.-J. Knowles, G. Knizia, F. R. Monby, M. Schülz *et al.*, MOLPRO, version 2012.1, a package of *ab initio* programs, 2012, see <http://www.molpro.net>.
- ³²T. H. Dunning, Jr., *J. Chem. Phys.* **90**, 1007 (1989).
- ³³T. Korona and H.-J. Werner, *J. Chem. Phys.* **118**, 3006 (2003).
- ³⁴K. Kaufmann, W. Baumeister, and M. Jungen, *J. Phys. B* **22**, 2223 (1989).
- ³⁵M. Allan, *J. Phys. B* **38**, 3655 (2005).
- ³⁶H. Kato, A. Suga, M. Hoshino, F. Blanco, G. García, P. Limão-Vieira, M. J. Brunger, and H. Tanaka, *J. Chem. Phys.* **136**, 134313 (2012).
- ³⁷H. Kato, K. Anzai, T. Ishihara, M. Hoshino, F. Blanco, G. García, P. Limão-Vieira, M. J. Brunger, S. J. Buckman, and H. Tanaka, *J. Phys. B* **45**, 095204 (2012).
- ³⁸H. Murai, Y. Ishijima, T. Mitsumura, Y. Sakamoto, H. Kato, M. Hoshino, F. Blanco, G. García, P. Limão-Vieira, M. J. Brunger, S. J. Buckman, and H. Tanaka, *J. Chem. Phys.* **138**, 054302 (2013).
- ³⁹P. Palihawadana, J. P. Sullivan, S. J. Buckman, Z. Mašín, J. D. Gorfinkiel, F. Blanco, G. García, and M. J. Brunger, *J. Chem. Phys.* **139**, 014308 (2013).
- ⁴⁰M. Fuss, A. Muñoz, J. C. Oller, F. Blanco, D. Almeida, P. Limão-Vieira, T. P. D. Do, M. J. Brunger, and G. García, *Phys. Rev. A* **80**, 052709 (2009).
- ⁴¹M. Fuss, A. G. Sanz, F. Blanco, P. Limão-Vieira, M. J. Brunger, and G. García, *Eur. Phys. J. D* **68**, 161 (2014).
- ⁴²F. Blanco and G. García, *Phys. Rev. A* **67**, 022701 (2003).
- ⁴³O. Zatsarinny, K. Bartschat, G. García, F. Blanco, L. R. Hargreaves, D. B. Jones, R. Murrie, J. R. Brunton, M. J. Brunger, M. Hoshino, and S. J. Buckman, *Phys. Rev. A* **83**, 042702 (2011).
- ⁴⁴M. Hoshino, M. Horie, H. Kato, F. Blanco, G. García, P. Limão-Vieira, J. P. Sullivan, M. J. Brunger, and H. Tanaka, *J. Chem. Phys.* **138**, 214305 (2013).
- ⁴⁵M. E. Riley and D. G. Truhlar, *J. Chem. Phys.* **63**, 2182 (1975).
- ⁴⁶X. Z. Zhang, J. F. Sun, and Y. F. Liu, *J. Phys. B* **25**, 1893 (1992).
- ⁴⁷G. Staszewska, D. W. Schwenke, D. Thirumalai, and D. G. Truhlar, *Phys. Rev. A* **28**, 2740 (1983).
- ⁴⁸F. Blanco and G. García, *Phys. Lett. A* **330**, 230 (2004).
- ⁴⁹A. Jain, *J. Phys. B* **21**, 905 (1988).
- ⁵⁰M. J. Brunger, L. Campbell, D. C. Cartwright, A. G. Middleton, B. Mojarrabi, and P. J. O. Teubner, *J. Phys. B* **33**, 783 (2000).
- ⁵¹M. J. Brunger, L. Campbell, D. C. Cartwright, A. G. Middleton, B. Mojarrabi, and P. J. O. Teubner, *J. Phys. B* **33**, 809 (2000).
- ⁵²A. Zecca, L. Chiari, A. Sarkar, and M. J. Brunger, *J. Phys. B* **41**, 085201 (2008).
- ⁵³A. R. Milosavljević *et al.*, *Eur. Phys. J. D* **40**, 107 (2006).
- ⁵⁴J. N. Bull, J. W. L. Lee, and C. Vallance, *Phys. Chem. Chem. Phys.* **16**, 10743 (2014).